Vacuum 206 (2022) 111487

Contents lists available at ScienceDirect

Vacuum

journal homepage: www.elsevier.com/locate/vacuum

Mechanically stable ultrathin flexible metallic Au/Pt/Au tri-layer as an alternative transparent conducting electrode for optoelectronic device applications

Reddivari Muniramaiah [a], Jean Maria Fernandes [a], M. Manivel Raja [b], Dilli Babu Padmanaban [c], P. Supraja [a], M. Rakshita [a], Nandarapu Purushotham Reddy [a], Gouranga Maharana [a], M. Kovendhan [d], Ganapathy Veerappan [e], Gangalakurti Laxminarayana [f], R. Rakesh Kumar [a], D. Haranath [a], D. Paul Joseph [a,*]

[a] Department of Physics, National Institute of Technology, Warangal, Telangana State, 506004, India
[b] Advanced Magnetic Group, Defence Metallurgical Research Laboratory, Kanchanbag, Hyderabad, Telangana, 500058, India
[c] Nanotechnology & Integrated Bio-Engineering Centre (NIBEC), Ulster University, Jordanstown, Newtownabbey, Co. Antrim, BT37 0QB, UK
[d] Department of Physics and Nanotechnology, SRM Institute of Science and Technology, Kattankulathur, Tamilnadu, 603203, India
[e] Centre for Solar Energy Materials, International Advanced Research Centre for Powder Metallurgy and New Materials (ARCI), Balapur, Hyderabad, Telangana State, 500005, India
[f] Research Centre Imarat (RCI), DRDO, Hyderabad, Telangana State, 500069, India

ARTICLE INFO

Keywords:
Ultrathin flexible film
TCEs
ACE
PEG
Au/Pt/Au tri-layer thin film

ABSTRACT

Indium tin oxide (ITO) is a ubiquitous transparent conducting oxide employed in several modern optoelectronic devices. However, due to limited availability and fast depletion of indium, there is an urge to supplement its use with suitable alternatives in appropriate sheet resistance range, depending on the application requirement. In this scenario, an alternative flexible transparent conducting Au/Pt/Au ultrathin metallic tri-layer electrode sputter-deposited on PET substrate is explored. The tri-layer shows maximum transmittance of 55% at 500 nm and it presents a nearly flat behavior in the entire visible spectrum. Electrical transport properties of Au/Pt/Au layer show sheet resistance of 66 Ω/□ and mobility of 8.32 $cm^2V^{-1}s^{-1}$, respectively. The contact angle measurement indicates that plain hydrophilic PET (62.6°) turns hydrophobic (94.2°) upon coating with Au/Pt/Au tri-layer. The surface properties analyzed using atomic force microscopy and optical profilometry indicate a crack-free, densely packed homogenous film. The tri-layer film shows mechanical stability up to 50,000 bending and twisting cycles. The obtained surface work function of Au/Pt/Au tri-layer film is 4.97 eV. The ultrathin flexible Au/Pt/Au tri-layer explored as top electrode in a piezoelectric generator and as top and bottom electrodes in an alternating current driven electroluminescent device exhibits appreciable performance.

1. Introduction

Flexible transparent conducting electrodes (TCEs) form the backbone of several modern optoelectronic devices such as building-integrated photovoltaics [1], flexible light-emitting diodes [2], organic light-emitting diode displays (OLEDs) [3], flexible photodetectors [4], foldable displays [5], electrochromic [6], piezoelectric generators [7], flexible electro-luminescent devices [8], etc. Most of these applications conventionally use indium tin oxide (ITO) as TCE due to its high optical transmittance (>85%) and low electrical sheet resistance (10–15 Ω/) [9]. However, the incessant use of ITO to meet the ever-growing energy demands has led to huge deficit of indium in the earth's crust, thereby adversely impacting the demand vs supply gap, especially in the prevailing pandemic due to enormous increase in the usage of display devices for academics, business, and in the entertainment sector. Moreover, the brittle nature of ITO, combined with the requirement of high annealing temperature (>400 °C), significantly impact its resistivity [10], restricting its applicability in emerging full-fledged flexible and stretchable optoelectronic devices. These limitations have led to considerable exploration of material alternatives to ITO for sustainable

* Corresponding author.
E-mail address: paul@nitw.ac.in (D.P. Joseph).

https://doi.org/10.1016/j.vacuum.2022.111487
Received 27 June 2022; Received in revised form 4 September 2022; Accepted 5 September 2022
Available online 13 September 2022

growth of the optoelectronics and energy related industries. These materials can be broadly classified as oxide and non-oxide-based TCEs [11]. Among non-oxide-based TCEs, several materials such as graphene [12], conductive polymers [13,14], carbon nanotubes [15], metal mesh [16], nanowires [17], etc. have been investigated as potential supplement to ITO due to their abundance, significant mechanical stability and considerable transparent conducting properties. Moreover, the use of some of these alternatives in large-area applications is restricted due to the high cost involved in mass production of these materials [18]. However, most of these materials do not possess high optical transmittance (due to non-existence of bandgap in some cases) and high electrical conductivity on par with that of the standard ITO, and hence, they cannot replace ITO but can only supplement to a greater extent.

Novel microstructures employing networks of metal nanowires and mesh patterns have been proposed for transparent conducting electrodes in order to overcome these shortcomings [11]. However, the major hinderances in their large-scale development are high optical haze due to scattering as well as electrical shorts from uneven surfaces, which are not desired for display-related applications [19]. Among the available alternatives, flexible ultrathin metal films are promising candidates in optoelectronics due to their facile and cost-effective fabrication methodology, high mechanical stability, considerable transparency and high electrical conducting properties.

In order to use metals as transparent electrodes, there are three major ways, firstly, metals can be patterned in a such a way that they can possess very high transmittance (>85%) as well as high conductivity [20–22]. This is also called as metallic grid, where the spacing between two grids will be the deciding factor for the values of resistance and transmittance of the film (However, issues like diffraction limit their applicability). Secondly, metallic nanowires can be randomly assembled for use as transparent conducting electrodes with much higher transparency (without the limitation of diffraction issues) [23–26]. Lastly, ultrathin metal films (~10 nm) can be deposited in the range of skin depth of the respective metal such that they give reasonably good transmittance without sacrificing the conductivity, and are suitable for establishing lower contact resistance for fabrication of devices [27,28]. In the case of metallic nanowires and metallic grids, the contact resistance will be a key factor. In some applications like display devices, the contact resistance must be minimal in order to have better contact and performance of the devices. In several cases, a single metal thin film layer is sandwiched between two dielectric layers to minimize haze and maintain significant transparency [29].

Ultrathin metallic films are usually adapted in a multilayer architecture so that the synergistic effect of each metal layer can enhance the overall transmittance and conductivity into a wider visible spectral range [30]. In a single layer, the transmittance maximum from individual metals is only limited to specific wavelengths [30]. The metals Au and Pt are low-reactive noble metals and their ultrathin films (below their respective skin depth) possess transmittance in the visible region of the electromagnetic spectrum [31]. In order to induce wide-range transparency in the visible region, their combination is made into a tri-layer architecture (Fig. 1a) and explored, thereby serving as motivation for the current work.

The thickness of individual layers based on their skin depth [32] forms the deciding factor for the transparent conducting property of multilayer TCEs. When the thickness of a thin film is high, its transmittance will be low, and when the thickness is low, the thin film possesses high transmittance. Hence, the thickness values of individual metal films become crucial when designing a TCE. In addition to this, the main advantage of using ultrathin metal films is their excellent flexibility, cost-effectiveness (due to lesser material usage), compactness, ease of deposition due to well-established physical vapor deposition techniques, and compatibility with a variety of substrates. As mentioned earlier, in some cases, a single metal thin film layer is sandwiched between two dielectric layers to minimize haze and maintain significant transparency [33]. Xiaoxiao et al. [34] reported that multi-layered ZnO/Au/ZnO has lower sheet resistance and higher transmittance than that of single ZnO layer of the same 50 nm thickness. Similarly, some of the oxide/metal/oxide sandwich structures have also been reported in literature [35–37]. The thin films can also be all-metal in a bilayer or tri-layer architecture, forming a TCE. Recently, an ultrathin all-metal tri-layer TCE with the configuration Au (2 nm)/Ag (4 nm)/Au (2 nm) deposited by thermal evaporation technique has been demonstrated [38]. A maximum of ≅ 62% optical transmittance (at 550 nm) was observed in this thermally-evaporated tri-layer, indicating a trade-off between optical transmittance and electrical conductivity [38]. Zhu et al. showed that the transmittance and sheet resistance of a continuous metal film composed of 6 nm Cr and 9 nm Au exhibits

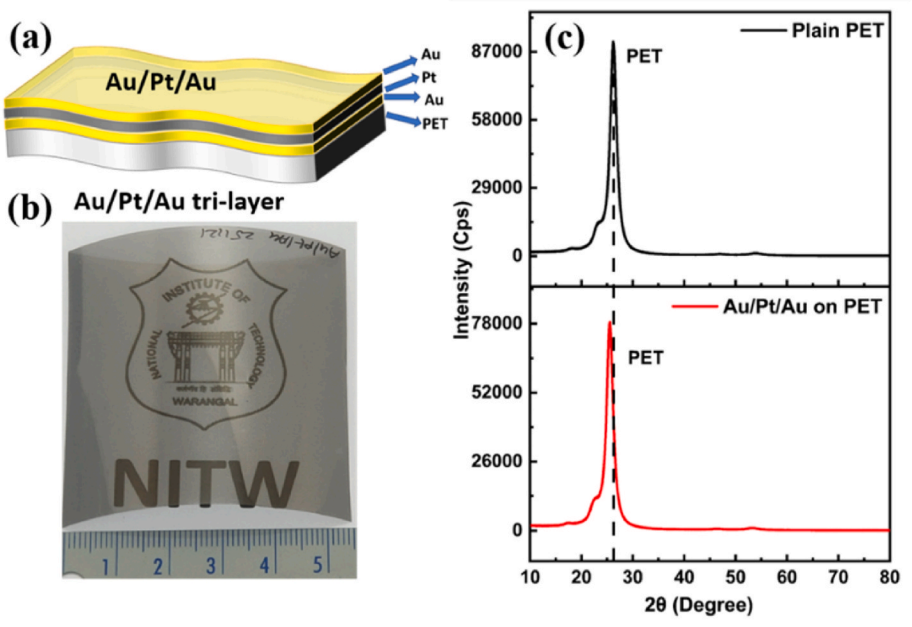

Fig. 1. (a) Pictorial 3D representation of ultrathin Au/Pt/Au tri-layer film architecture, (b) Photograph of deposited homogenous tri-layer indicating its bendable and transparent nature, and (c) X-ray diffraction patterns of plain PET and Au/Pt/Au sputter deposited over PET film.

slightly better transmittance with a sacrificial loss in conductivity compared to the films with higher thickness of Au (17, 26, and 34 nm), but it displays very high resistance of 766 kΩ/. However, in the case of metal mesh electrodes with Au thicknesses of 17, 26, and 34 nm, decrease in sheet resistance is observed with increased metal thickness without appreciable change in the film transmittance, mainly due to the apertures in the film [39]. Such network kind of films are not suitable for all types of optoelectronic devices, due to non-uniform surface work function by the presence of apertures. The deposition methods used to fabricate these structures also play a vital role in influencing their optical and electrical properties. Metal-based TCEs are predominantly deposited using magnetron sputtering due to its capability to produce high quality films even over a larger area [40].

In the case of metallic thin films, it is challenging to stabilize both conductivity and transmittance since thick films show very good conductivity, but very low transmittance. The total thickness and individual metal skin depth of the film decide the combined transparency and electrical conductivity. In this regard, the effective skin depth (δ_{eff}) of the Au/Pt/Au tri-layer film at $\lambda = 500$ nm is calculated using a MATLAB code based on a theoretical model by Deng et al. [38,40] as shown in the following equations:

$$\delta_{eff} = \sum_{i=1}^{N+1} d_i, \quad i = 1,\ 2,\ ----,N,\ N+1 \tag{1}$$

where,

$$d_i = \int_{\sum_{j=0}^{i-1} t_j}^{\sum_{j=0}^{i} t_j} \left[\frac{\prod_{j=0}^{i-1}(1+\Gamma_j)}{\prod_{j=0}^{i}\left(e^{\gamma_j t_j} + \Gamma_j e^{-\gamma_j t_j}\right)} \left(e^{-\gamma_i \left(z - \sum_{j=0}^{i-1} t_j\right)} + \Gamma_i e^{\gamma_i \left(z - \sum_{j=0}^{i} t_j\right)} \right) \right] \tag{2}$$

$$\text{Propagationconstant}\ \ \gamma_i = (1+j)\sqrt{\frac{\omega \mu_i \sigma_i}{2}} \tag{3}$$

$$\text{Reflection}\ \ \text{co}-\text{efficient}\ \ \Gamma = \frac{n_1 - n_2}{n_1 + n_2} \tag{4}$$

where, t is thickness of the layer, ω is the angular frequency of visible light, μ is the permeability of the layer, σ is the electrical conductivity, n_1 and n_2 are refractive indices of ith and $(i+1)^{th}$ layers, respectively. The iterated value of δ_{eff} using Eq. (1) for the Au/Pt/Au tri-layer film is 7.957 nm. The critical requirements of electrodes in flexible optoelectronic and wearable electronic devices are good visible-light transmittance, electrical conductivity and adaptiveness to mechanical changes such as bending, folding and twisting. In the current work, we explore the use of relatively low-reactive noble metals such as Au and Pt in a tri-layer architecture deposited on a flexible PET substrate for use as a TCE. Pt has good chemical stability and stable temperature co-efficient of resistance [41] and Au is also a typical metal for serving as stable electrode [42]. Each layer with a thickness of 2 nm (based on the skin depth as estimated using the above equations) is deposited on a flexible PET film using sputtering technique in Au/Pt/Au architecture. Au metal is coated as seed layer as well as capping layer to decrease the surface/interface roughness and to protect the Pt layer from oxidation, and it also helps to increase the conductivity of the ultrathin film. The flexibility and transparent conducting properties of this TCE are explored and demonstrated in piezoelectric nanogenerator (PEG) and alternating current electroluminescent (ACEL) devices as a proof of principle validation of its viability in a variety of optoelectronic device applications.

2. Experimental details

2.1. Materials

A substrate of thickness >120 μm results in poor flexibility in general, and therefore, a highly flexible poly-ethylene terephthalate (PET) substrate of 35 μm thickness was used as substrate. High purity Au and Pt metal targets were used to deposit the tri-layers in a LJ5 ultra high vacuum (UHV) DC magnetron sputtering system. Zinc nitrate [$Zn(NO_3)_2$], NaOH pellets of AR grade chemicals purchased from Sigma Aldrich, USA, and aluminum foils of thickness ≅ 0.1 mm purchased from Special Metals Pvt. Ltd., India, were used to prepare the ZnO film during device fabrication. $ZnCl_2$, $MnCl_2$, and NH_4OH of AR grade chemicals (Sigma Aldrich, USA) were used to prepare ZnS:Mn phosphor material for fabricating the devices.

2.2. Deposition of metallic tri-layer film on PET

The PET film was cleaned using isopropanol (IPA) and a jet of inert gas prior to deposition to remove dust particles clinging to the surface of the substrate. Multi target (5 Nos.) ultra-high vacuum (UHV) DC magnetron sputtering equipment was used for deposition of the multi-layer using Ar gas. The Au/Pt/Au multi-layer was deposited sequentially using high purity (99.9 wt%) Au and Pt sputtering targets. The sputtering was performed in confocal geometry with an incident angle of 45°. The substrate was rotated at 10 RPM during deposition for achieving uniform thickness. The metallic tri-layer (Au/Pt/Au) film was deposited in ultra-high vacuum (6×10^{-8} Torr) with substrate temperature maintained at 70 °C. The thickness of each layer is 2 nm and the total thickness of the Au/Pt/Au film is 6 nm. The optimization details of individual metal thickness by X-ray reflectivity (XRR) (Rigaku Smart Lab multipurpose) are given in the supplementary information. Thickness values were calibrated using XRR, where Figs. S1 and S2 correspond to Au and Pt, respectively (Table S1). All the layers were deposited by supplying input sputtering power of 25 W under Ar gas with a working pressure of 5 mTorr. The seed and capping Au layers were deposited with 2 nm thickness for 34 s with a deposition rate of 0.058 nm/s. The Pt layer with a thickness of 2 nm was deposited at a deposition rate of 0.028 nm/s for 72 s (Table S2). Fig. 1a shows the 3D (Fig. S3 shows 2D) pictorial representation of the deposited Au/Pt/Au tri-layer. Fig. 1b shows the photograph of the sputter-deposited Au/Pt/Au tri-layer on flexible PET film.

2.3. Fabrication of piezoelectric generator

The Au/Pt/Au sputter-deposited ultrathin flexible film and aluminum foil were used as top and bottom conducting electrodes, respectively, in the fabrication of a piezoelectric nanogenerator (PEG). ZnO film was deposited on aluminum foil by chemical bath deposition method. An aqueous solution of 160 ml was prepared using 0.5 g zinc nitrate and 0.3 g of sodium hydroxide pellets dissolved in DI water. The aluminum foil was cleaned with acetone and dipped into the solution, after which it was treated in a vacuum oven for 4 h at 80 °C to facilitate the growth of ZnO nanorods over the aluminum foil. The ZnO grown on aluminum foil was cleaned with DI water to remove loosely bound ZnO nanostructures. The aluminum foil with ZnO nanorods was fixed firmly to the flexible Au/Pt/Au ultrathin film using Kapton tape without any short circuit of the electrodes. The piezo-output response was obtained from a digital storage oscilloscope (DSO) (Tektronix-TBS 1102) interfaced with a computer by applying finger-tapping pressure. The switching-polarity measurements were also performed by interchanging the electrode connections.

2.4. Fabrication of alternating current electroluminescent device

The orange emitting ZnS:Mn phosphor material was prepared using

an alkaline technique [43]. Ammonia complex formed by the reaction of $ZnCl_2$ with NH_4OH was subsequently exposed to H_2S gas bubbles to obtain ZnS precipitate which is found to be luminescent. Manganese (II) chloride ($MnCl_2$), a soluble dichloride salt of manganese was then added to ZnS precipitate in ppm increments and dried in an oven at 120 °C/5 h. The obtained precursor was thoroughly ground with a mortar and pestle, and then fired at 950 °C in sulphur atmosphere for 43 h to obtain ZnS:Mn (0.01 wt % of Mn) phosphor for use as an active layer in an ACEL device. The final ZnS:Mn phosphor material was thoroughly mixed with a dielectric medium ($\varepsilon_r \cong 5$) to obtain the ZnS:Mn paste.

Two ultrathin Au/Pt/Au metal-coated PET films as the top and bottom transparent conducting electrodes, and an orange emissive layer of ZnS:Mn layer sandwiched in the middle [44–47] were used to assemble the ACEL device. The bottom electrode was covered with double-sided transparent tape, and the middle of the tape was engraved by cutting into a rectangular well shaped pit. Then, the ZnS:Mn emissive paste was filled in the rectangular well on the bottom ultrathin flexible Au/Pt/Au film by doctor blade technique [44]. Another ultrathin flexible Au/Pt/Au film as top electrode was attached to the emissive layer without any electrical short circuit with the bottom electrode. Double side glued copper tape was affixed to the top and bottom electrodes to clip to the power source without puncturing the electrodes. A cost-effective indigenous portable power source was designed to energize the device by transforming direct current field into an alternating current field. The input voltage of this source can be varied between 12 and 300 V_{AC} using a potentiometer.

2.5. Characterization

The Rigaku Smart Lab automated multipurpose X-ray diffractometer with Cu Kα radiation (wavelength, $\lambda = 1.5406$ Å) was used to analyze the structural properties. Individual layer thickness was optimized using X-ray reflectivity technique prior to deposition. Transmittance spectra were obtained using a UV–vis spectrometer (Analytik Jena, SPECORD 210 PLUS). Surface morphology and elemental composition were analyzed using a scanning electron microscope (Tescan, Vega 3 LMU). Surface topography was obtained from a non-contact optical profiler (NanoMap 1000WLI). The surface features of the films deposited on glass substrates were explored using atomic force microscopy (AFM, Park NX_{10}). Contact angle measurements were performed using DSA25 Drop Shape Analyzer (KRUSS, Germany). Electrical transport properties were measured using linear four-probe and Hall effect (Ecopia, HMS 3000) techniques. Work function of the samples was measured using Kelvin probe microscopy (KP Technologies APS04) operated in air with a 2 mm gold alloy tip. Bending and twisting tests were performed to check the flexibility of the Au/Pt/Au film using an indigenous bending and twisting apparatus [32]. Using Olympus (Model BX53F) optical microscope in reflection mode, the surface features of the deposited Au/Pt/Au tri-layer film were explored before and after inducing fatigue by the bending-twisting apparatus. To study the adhesion properties, scotch tape test was performed on the surface of the film. However, scotch tape test is only qualitative in nature, but is very important in evaluating the strength and quality of film adhesion, especially for a 6 nm multilayer film.

3. Results and discussion

3.1. Structural properties

X-ray diffraction patterns of plain PET and Au/Pt/Au coated PET are shown in Fig. 1c. Both the patterns are nearly similar, however, the main peak around 26.19° corresponding to PET substrate is shifted to 25.54° after deposition of Au/Pt/Au layers. This information gives an indication about the existence of the deposited Au/Pt/Au metallic tri-layers over the PET substrate. No individual peaks corresponding to Au and Pt are observed since the total thickness of the tri-layer is merely 6 nm, and moreover, since the deposition temperature is only 70 °C, the deposited layers may be amorphous in nature.

3.2. Surface topology

Surface topography of the sputtered Au/Pt/Au tri-layer on PET film is analyzed using AFM and optical profiler techniques. The surface analysis of the flexible Au/Pt/Au sputtered PET film is highly challenging since the tip of the AFM instrument is extremely sensitive. Therefore, in the present work, the Au/Pt/Au tri-layer was sputter-deposited simultaneously on both glass and PET substrates. Moreover, metal films over 100 nm thickness are not beneficial for use in optoelectronic devices which essentially require a smooth electrode surface [48]. The 2D and 3D AFM images (Fig. 2a and b) of Au/Pt/Au tri-layer on glass substrate show that the film is crack-free and densely packed. From Fig. 2b, the Au/Pt/Au thin film clearly indicates the presence of needle-like particulates on the surface of the film with a lower RMS roughness of 1.04 nm. The topography of the flexible Au/Pt/Au sputtered on PET film was analyzed using optical profiler in non-contact mode and the 2D and 3D images are shown in Fig. 2c and d, respectively. Fig. 2(e and f), shows the 2D and 3D images of plain PET surface and it is observed to be smooth. Also, the surface roughness calculated using AFM was reported to be 3.68 nm by K.G. Kostov et al. in the literature [49]. The 3D image of Au/Pt/Au film clearly shows a highly homogeneous film with significantly less spike-like features at that magnification over a larger area (1 mm × 1 mm), which implies its suitability in large-scale optoelectronic devices.

In the present case, the ultrathin tri-layer is deposited by sputtering technique for an individual layer thickness of 2 nm. Here, the most probable mode is Stranski-Krastanov, which is a mixed layer plus island growth mode [50,51]. Therefore, within a threshold limit, island formation may occur and upon depositing the Pt and Au overlayers, a considerably sharp interface exists, as evident from the X-Ray reflectivity data (Please see the supplementary file) and also from the interference pattern obvious in the UV–Vis transmittance data (Please see inset of Fig. 4b). Therefore, the deposited ad-atoms or molecules are strongly bonded to the substrate and to each other progressively with the deposition of subsequent layers. All these factors lead to considerably uniform film formation with a moderate surface roughness of 1.04 nm.

3.3. Wettability of the Au/Pt/Au ultrathin flexible film

The wettability nature of the sputter-deposited Au/Pt/Au ultrathin flexible film is analyzed using contact angle measurement with de-ionized water as test medium. In 1805, Young defined a relation between three interfacial energies per unit area [solid-vapor interface (γ_{sv}), solid-liquid interface (γ_{sl}), and liquid-vapor interface (γ_{lv})]. Young's relation is given as follows [52],

$$\Upsilon_{sv} = \Upsilon_{sl} + \Upsilon_{lv} \cos\theta \tag{5}$$

where, θ is the angle between the solid surface and the tangent of the liquid drop at the contact point between the three phases. Based on the contact angle of water, the wettability nature of the thin film surface is divided into three categories: non-wettable (hydrophobic) ($\theta > 90°$), partially wettable (hydrophilic) ($0° < \theta < 90°$), and totally wettable ($\theta = 0$) (super hydrophilic) [52]. Usually, the contact angle of a thin film is mainly dependent on aspects such as surface roughness, functional groups existing on the surface of the film, impurities present on the film's surface, porosity of the film, and surface energy [53].

In the present case, de-ionized water droplets tested on plain PET, Au/Pt/Au sputtered deposited over PET and commercial ITO films are shown in Fig. 3a, b and 3c, respectively. The plain PET substrate shows hydrophilic nature with a contact angle of 62.6°, and after deposition of the Au/Pt/Au metallic tri-layer, it turns hydrophobic with a contact

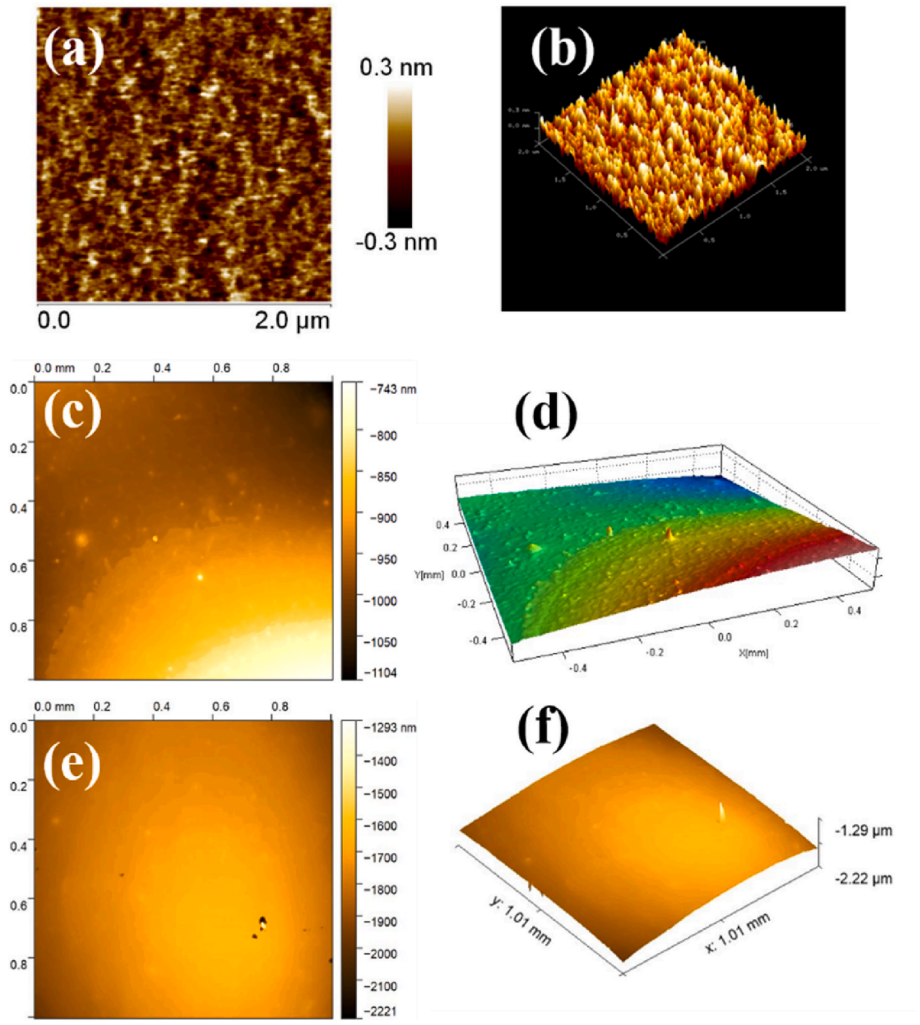

Fig. 2. (a and b) The 2D and 3D AFM images of Au/Pt/Au tri-layers deposited on glass substrate, (c and d) the 2D and 3D optical profiler images of Au/Pt/Au tri-layer deposited on PET substrate, and (e and f) 2D and 3D optical profiler images of plain PET film.

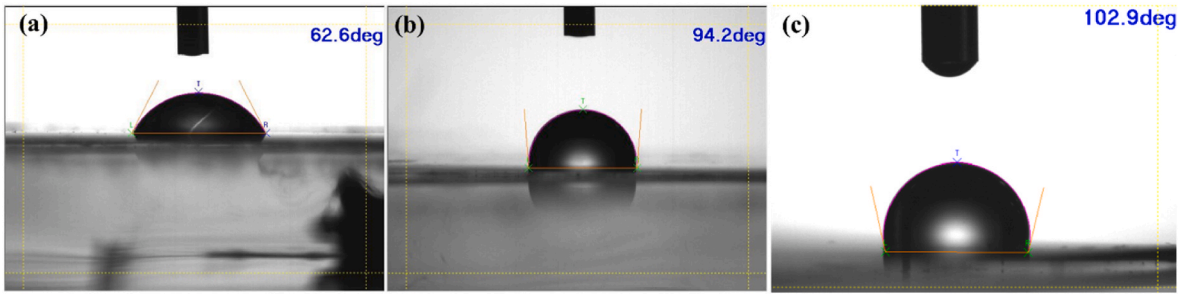

Fig. 3. Contact angle measurement of water droplet on the surface of (a) Plain PET, (b) Au/Pt/Au tri-layer film coated over PET, and (c) Flexible commercial ITO.

angle of 94.2°. Here, the variation in the contact angle is mainly due to surface roughness and chemical nature of the film. The low surface roughness (1.04 nm) of the deposited ultrathin flexible Au/Pt/Au film with nano-dimensional needle-like features may be the cause for the change from hydrophilic to hydrophobic nature. The commercial flexible ITO also shows hydrophobic nature with a contact angle of 102.9°. Hydrophobic nature of the deposited thin film helps in low-wetting of the Au/Pt/Au ultrathin film, which may be useful for self-cleaning-like requirements of the deposited film.

3.4. Optical transmittance

Fig. 4a shows the optical transmittance spectra of the deposited Au/Pt/Au tri-layer and commercial flexible ITO film (Zhuhai Kaivo Optoelectronic Technology Co., China). The Au/Pt/Au tri-layer film shows a maximum transmittance (*T*) of 55% at 500 nm, whereas flexible ITO has slightly higher transmittance of 58% at 550 nm. The transmittance of commercial ITO is marginally higher in the visible region, but in the case of the deposited Au/Pt/Au ultrathin flexible film, the transmittance shows near-flat behavior in the entire spectrum (350–1000 nm). However, this is lower than that of the Au/Ag/Au tri-layer (62%) [38] and

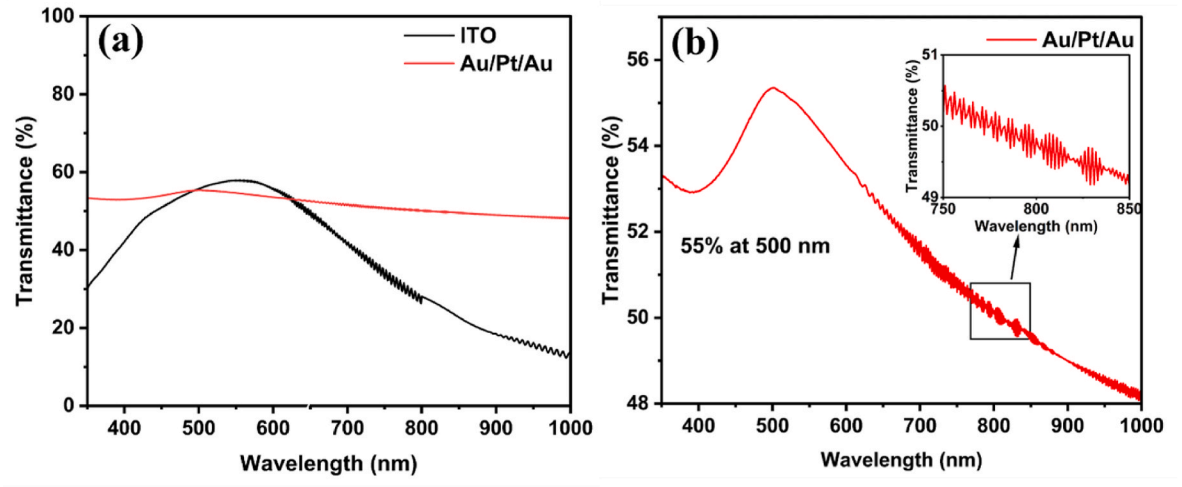

Fig. 4. (a) Transmittance spectra of Au/Pt/Au coated PET and commercial flexible ITO films, and (b) Enlarged transmittance spectra of the Au/Pt/Au flexible ultrathin metal film (inset is the interference pattern due to the constituent layers of the tri-layer architecture).

higher than the reported value for Cu/Ag/Au tri-layer film (40%) [54] deposited by thermal evaporation technique. Alexander et al. reported the individual transmittance of 2 nm Au thin film deposited on glass substrate to be 70% at 500 nm [30,55]. In the present case, the addition of another 2 nm of Pt and 2 nm of Au leads to decrease in the transmittance of the deposited Au/Pt/Au layer. However, the transmittance of the deposited Au/Pt/Au flexible thin film shows an extended behavior from ultraviolet region to near-infrared region, with a value ranging between 48% and 55% (Fig. 4b). The flat behavior in the transmittance spectra is mainly due to the presence of two different metal layers (Au and Pt) in the tri-layer architecture, demonstrating significant change in transparency in comparison with that of commercially available flexible ITO from ultraviolet to near-infrared regions. The peak at 500 nm with transmittance value of 55% is mainly due to the presence of Au layer in the tri-layer architecture [30]. The inset of Fig. 4b shows an interference pattern around 800 nm, which is due to the layered structure of the sample with distinct and sharp interface. From the literature, it is well known that ITO and FTO films present very low transmittance in the near-infrared and infrared regions, which is mainly due to the presence of free electron plasmon resonance or strong free carrier absorption [56–59]. The optical transparency of the ultrathin Au/Pt/Au metal film dominates that of ITO in the near-infrared region, which may be due to the presence of free-carrier plasmon edge in the infrared region [59]. However, the transmittance of an ultrathin film is mainly dependent on its percolation threshold thickness of the respective material [60]. When the thickness of the film is below the percolation threshold, it forms a network of islands, whereas an increase in film thickness leads to continuous film formation, resulting in reduced transparency [60].

3.5. Electrical transport properties

The electrical transport properties of the Au/Pt/Au tri-layer film are evaluated using Hall effect at room temperature (300 K). The carrier concentration (N), sheet resistance (R_s), resistivity (ρ), conductivity (σ) and mobility (μ) values of Au/Pt/Au and commercial ITO are listed in Table 1. At lower thickness, below the threshold limit, due to island like features leading to discontinuity may result in higher electrical resistance. If the thickness of the film surpasses the percolation threshold, then the discrete metal clusters further grow, forming a continuous metal layer, thereby increasing the conductivity of ultrathin metal films [61]. In the present case, 2 nm Au is deposited as seed layer to deposit Pt layer of 2 nm, followed by 2 nm of Au layer as capping layer in order to avoid oxidation and for better chemical stability and surface functionality. The deposited Au/Pt/Au layer shows a sheet resistance of 66 Ω/□ with resistivity of 3.72×10^{-5} Ωcm, which is slightly higher than that of commercial flexible ITO film.

The resistivity of ultrathin Au/Pt/Au metal film is severely affected by electron scattering from grain boundaries and interfaces. The charge carrier concentration and conductivity of the deposited Au/Pt/Au ultrathin metal are marginally higher than that of commercial ITO (Table 1). The mobility of the deposited film shows slightly lower (8.32 $cm^2V^{-1}s^{-1}$) value than that of commercial ITO (10.18 $cm^2V^{-1}s^{-1}$), which may be due to the carrier scattering process that occurs in the thin film due to grain boundary scattering, phonon scattering and free carrier trapping at the interfacial defects [63]. The presence of a greater number of charge carriers leads to more frequent collisions, resulting in a decrease in the mean free path of electrons, in turn, contributing to lower mobility of the Au/Pt/Au ultrathin metal film. In addition to this, the surface features of the film also affect the mobility of carriers in the deposited film.

3.6. Surface work function

Surface work function (ϕ) plays a very important role in the efficiency and performance of optoelectronic devices. Here, the work function of the sputtered Au/Pt/Au ultrathin flexible thin film is estimated from Kelvin probe measurement operated in ambient atmosphere with a 2 mm gold alloy tip [64]. Initially, the gold tip is calibrated with a

Table 1
Optoelectronic parameters of Au/Pt/Au ultrathin flexible tri-layer film in comparison with ITO and previously reported metallic tri-layer film.

Sample name	$N(cm^{-3})$	$R_s(\Omega/\square)$	$\rho(\Omega cm)$	$\mu(cm^2V^{-1}s^{-1})$	$T(\%)$	$\Phi(eV)$	$FoM(\Omega^{-1})$	Ref
ITO	1.29×10^{22}	5	4.73×10^{-5}	10.18	≅ 55 (500 nm)	4.4	5.06×10^{-4}	[38]
Cu/Ag/Au[a]	1.15×10^{23}	7.7	9.70×10^{-6}	5.58	≅ 40 (550 nm)	–	1.39×10^{-5}	[62]
Au/Ag/Au[a]	2.48×10^{23}	10.42	7.46×10^{-6}	3.4	≅ 62 (550 nm)	–	5.20×10^{-4}	[38]
Au/Pt/Au[b]	2.01×10^{22}	62.08	3.72×10^{-5}	8.32	≅ 55 (500 nm)	4.97	3.39×10^{-5}	Present work

[a] : thermal evaporation.
[b] Sputtering (Present work).

standard Au-coated Al substrate (work function of Au-coated Al substrate is 5.1 eV) by evaluating the contact potential difference (V_{CPD}) between the Au film and the tip [64].

$$\Phi_{tip} = \Phi_{Au\ coated\ Al\ substrate} - V_{CPD} \quad (6)$$

$$\Phi_{tip} = 5.1 - V_{CPD} \quad (7)$$

The value Φ_{tip} is estimated (from equation (7)) to be 4.877 ± 0.016 eV. The Au/Pt/Au ultrathin flexible film is then loaded, and V_{CPD} between the sample and the tip is calculated using the following relation [64].

$$\Phi_{Au/Pt/Au} = \Phi_{tip} + V_{CPD}\ (\text{Au/Pt/Au}) \quad (8)$$

The estimated work function of the sputter-deposited Au/Pt/Au ultrathin flexible film is found to be 4.97 eV. The work function values of individual Au and Pt metals are reported to be in the range 5.31–5.47 eV and 5.12–5.93 eV, respectively [65]. The reported work function for ITO is around 4.3–4.4 eV [66–69]. Although the measured work function of Au/Pt/Au ultrathin flexible film is higher than that of ITO, it can be employed in specific applications, wherever this range of work function is necessary. Nevertheless, many optoelectronic devices need at least one electrode with a low surface work function. Low surface work function improves either the collection of electrons or the injection of electrons from the conduction band minima (CBM) or lowest unoccupied molecular orbital (LUMO) of a given inorganic/organic semiconductor.

3.7. Mechanical stability

The development of flexible electronic gadgets for portable and wearable devices requires a variety of transparent conducting flexible electrodes with good stability for several bending and twisting cycles without significant change in sheet resistance, so as to retain the efficiency and lifetime of the device. Therefore, it is necessary to study the stability of sheet resistance of the sputter-deposited Au/Pt/Au ultrathin flexible electrode for thousands of bending and twisting cycles, which shows the ability of the films to withstand external stress and strain. The bending and twisting tests of commercial ITO along with Au/Pt/Au ultrathin flexible film were performed using an indigenously designed apparatus employing an ATmega328 microcontroller [38]. Insets of Fig. 5a and b shows the films loaded in bent and twisted positions, respectively. The bending and twisting tests were performed at a speed of 20 bending cycles per min and 14 twisting cycles per min, respectively. The time taken for 5000 bending and twisting cycles was 250 and 350 min, respectively. Sheet resistance stability measurements of total 50,000 bending (Fig. 5a) and twisting (Fig. 5b) cycles each with steps of 5000 bends and twists were performed on the sputtered Au/Pt/Au ultrathin flexible tri-layer film. The sheet resistance stability measurement of commercial flexible ITO was also performed at the same rate. Due to lower stability, a total number of 2500 bending and twisting cycles with an interval of 500 cycles were performed.

The bending and twisting-induced strain in a metallic thin film is dependent on the thickness of the metallic film (d_m), thickness of the substrate (d_s), bending radius (R), and Young's modulus of the deposited metal (γ_m) and substrate (γ_s) [70]. The strain in the deposited film can be calculated using the following equation [70].

$$S = \left(\frac{d_m + d_s}{2R}\right)\left(\frac{1 + 2\eta + \chi\eta}{(1+\eta)(1+\chi\eta)}\right) \quad (9)$$

where χ is the ratio of Young's modulus of the deposited metal to that of the substrate, and η is the ratio of metal film thickness to substrate thickness. From the equation, the bending strain is proportional to the thickness of the deposited film, and so, if the thickness of the film is reduced, the bending strain of the film decreases, leading to increase in the flexibility and stability of the deposited metal film.

Metal films are highly ductile and can withstand up to several thousands of bending and twisting cycles. Yin et al. demonstrated good stability of a flexible OLED fabricated using Ag (80 nm) as anode with bending radius of 30 μm, without degrading the device performance [71]. Kang et al. reported a polymer-metal hybrid electrode which showed good stability up to 1000 bending cycles compared to commercial ITO, and they observed decrease in device performance for the ITO electrode after 1000 bending cycles, whereas the device made with Ag electrode showed nearly no degradation of device performance [14]. A comparison between previously reported alternative flexible transparent conducting electrodes with the present work is given in Table 2.

Au/Pt/Au ultrathin flexible film with a thickness of 6 nm shows good mechanical stability up to 50,000 bending and twisting cycles. The flexibility of the Au/Pt/Au film is 100 times higher than that of the commercial flexible ITO as shown in Fig. 5a and b. The flexible ITO film is not stable even up to 2500 bending and twisting cycles as shown in Fig. 5a and b, causing damage due to its brittle nature. The observed high stability in Au/Pt/Au film is mainly due to the ductile nature of metallic layers compared to that of oxide films, and also because of low thickness of the Au and Pt layers.

The sheet resistance of Au/Pt/Au ultrathin flexible film does not exceed 300 Ω/□ even after 50,000 bending and twisting cycles, whereas

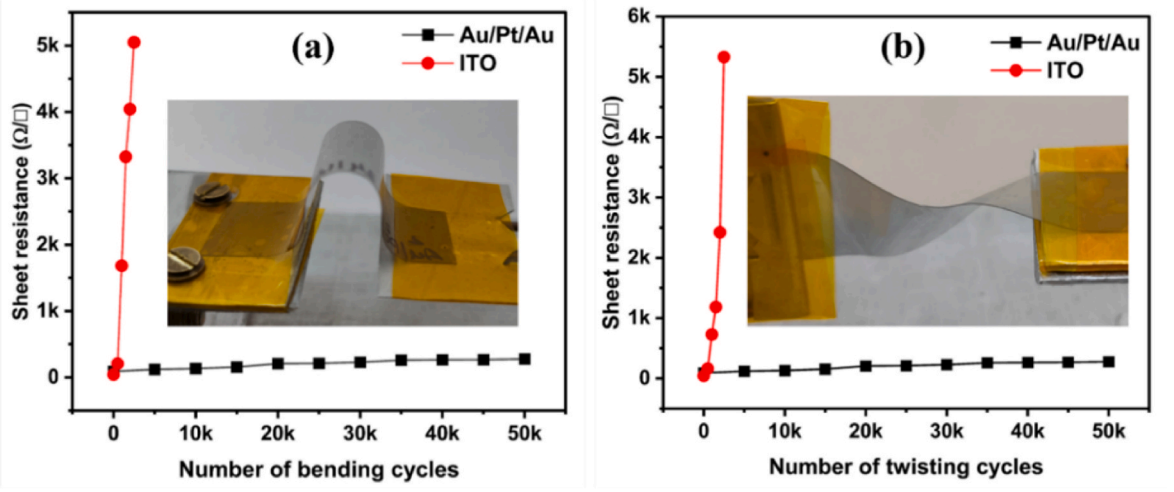

Fig. 5. Stability of sheet resistance of Au/Pt/Au tri-layer film in comparision with commercial ITO for (a) bending and (b) twisting modes (Insets are the photograph of the respective modes).

Table 2
Comparison of parameters of Au/Pt/Au tri-layer film to previously reported alternative transparent conducting electrodes.

Material	Thickness (nm)	T (%)	R_s (Ω/□)	Flexibility (bending cycles or radius)	Application	Ref.
Ag NWs	30	~85	50	1–5 mm	ACEL	[72]
ZnO/Cu/ZnO	6.5	84	20	0–12 mm	OPV	[73]
Ta_2O_5/Al-doped Ag	4	75	46.8	200	OPV	[74]
Au	4.4	78.4	70.4	2000	OLED	[75]
Au	7	72	24	1000	OLED	[76]
Au	7	75	19	2000	OLED	[77]
Ag	12	69	10	1000	OPV	[78]
Au	6	28	766	3000	OLED	[39]
ITO	≅ 100	55	5	2500	–	Present work
Au/Pt/Au	6	55	62	50000	PEG & ACEL	

in the case of commercial flexible ITO, it exceeds 300 Ω/□ within 500 bending and twisting cycles, and drastically increases to 5 kΩ/□ within 2500 bending or twisting cycles (Fig. 5a and b). Fig. 6 shows the optical microscopic images of commercial ITO film before and after 2500 bending and twisting cycles, where cracks on the ITO film are observed clearly. These cracks lead to discontinuity in the film surface, resulting in high sheet resistance.

Whereas, in the case of sputter-deposited Au/Pt/Au ultrathin flexible film, optical microscopic images before and after 50,000 bending and twisting cycles are shown in Fig. 6d–f. Fig. 6e and f shows few cracks even after 50,000 bending and twisting cycles. However, these small cracks do not have much effect on the sheet resistance of the Au/Pt/Au ultrathin film. In addition to flexibility, it is necessary to investigate the adhesion properties of the deposited Au/Pt/Au ultrathin flexible film by subjecting it to scotch tape test. A scotch tape was placed and pressed on the film's surface, and then stripped away manually for about six trials. Upon visual inspection, the film was found to be intact, implying good adhesion, and the film was also electrically conducting as tested for its electrical continuity using a multimeter with almost no change observed in the sheet resistance after the tape test. All these properties suggest that the Au/Pt/Au ultrathin tri-layer is a promising and electrically stable candidate for appropriate flexible optoelectronic device applications with long-term robustness.

3.8. Piezoelectric nanogenerator

Fig. 7a shows the schematic representation of a piezoelectric nanogenerator (PEG) device architecture. Fig. 7b shows flower-like morphology of the near-vertically grown ZnO nanostructures and Fig. 7c shows the elemental composition of the same. To measure the open-circuit voltage of the nanogenerator, the bottom aluminum foil (Al) electrode and the top Au/Pt/Au ultrathin flexible electrode are both connected to a DSO using probes. In the forward connection, the top electrode (Au/Pt/Au ultrathin flexible film) is connected to the positive probe of DSO, and the bottom Al electrode is connected to the negative probe of the DSO. When a force is applied to the device by finger tapping, piezoelectric output voltage is generated due to mechanical deformation of the ZnO nanostructures. The generated output voltage for the repeated finger tapping is recorded in the DSO. The output voltage of the device is also measured in reverse connection, which is called the switching-polarity test. The switching-polarity test confirms that the output voltage is actually due to the nanogenerator device, and not from any spurious signals/instrument noise. The maximum output voltage (in both forward and reverse bias) produced for each finger tap by the nanogenerator device is ≅ 150 mV, as shown in Fig. 7d. The generated output voltage is nearly at the same level as that of the commercial ITO/PET and copper electrode-based ZnO nanogenerators reported previously [79,80]. The use of Au/Pt/Au ultrathin tri-layer as a top electrode makes the device very compact and flexible. Moreover, transparency of the top electrode contributes to additional degree of freedom which may be beneficial to induce novel functionality through interaction with incident light radiation.

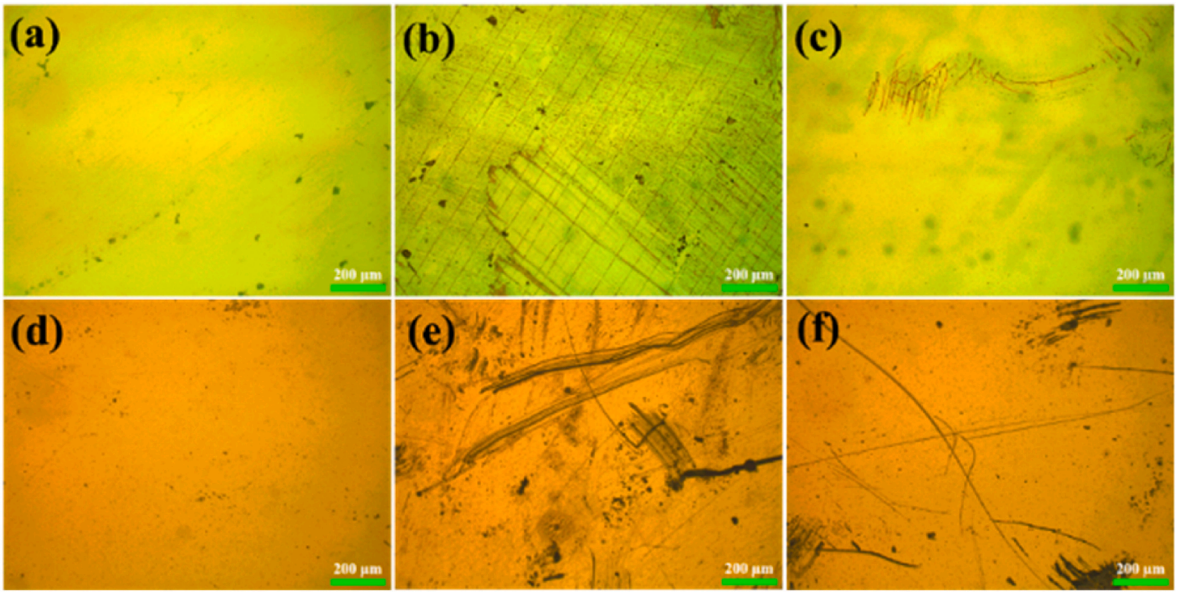

Fig. 6. Microscopic images of commercial flexible ITO film: (a) pristine, (b) after 2500 bending cycles, (c) after 2500 twisting cycles; and Au/Pt/Au tri-layer coated over PET: (d) pristine, (e) after 50000 bending cycles, (f) after 50000 twisting cycles.

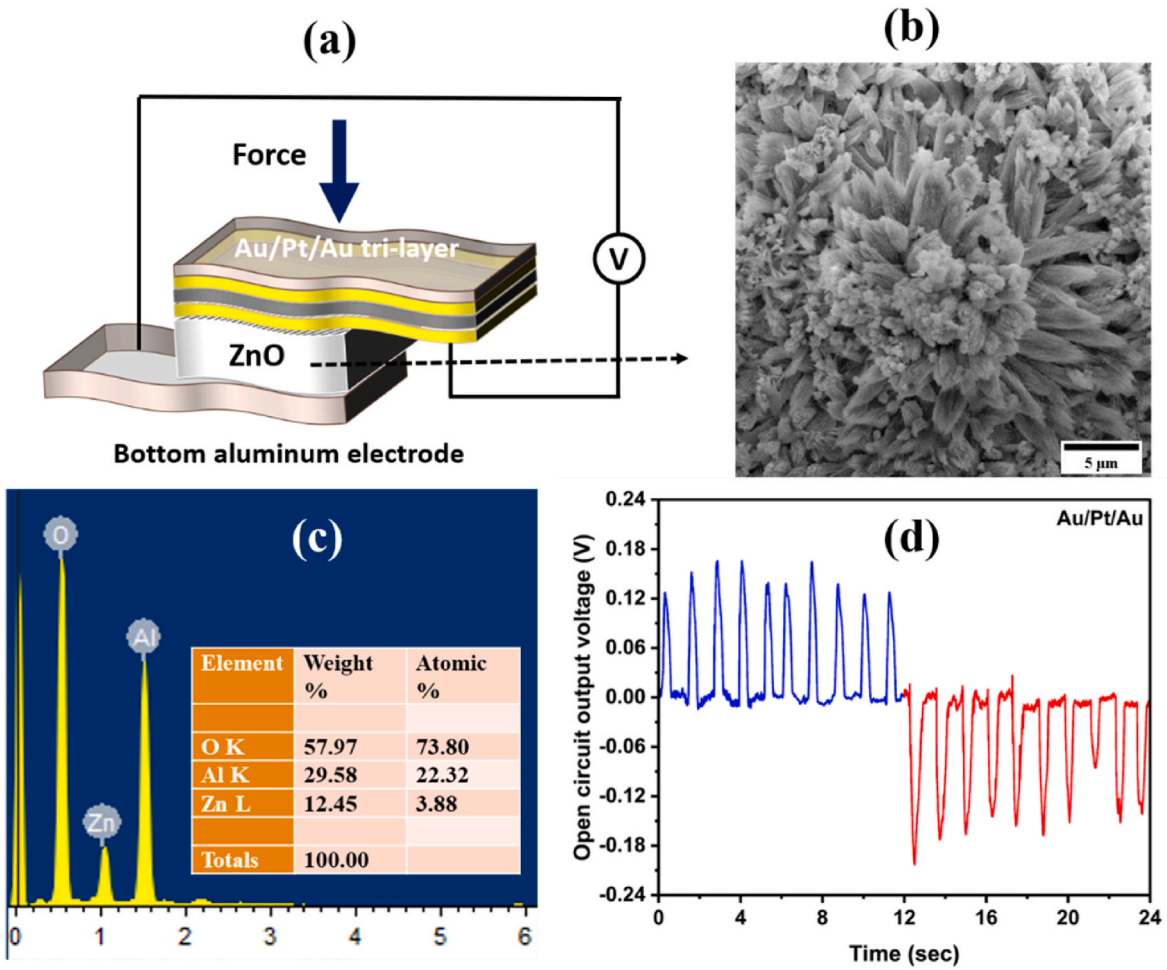

Fig. 7. (a) Piezoelectric generator device architecture with Au/Pt/Au flexible transparent thin film as a top electrode, (b) SEM image, (c) EDAX spectrum of ZnO grown on aluminum foil (inset is the weight and atomic percentage table) and (d) Time vs Open circuit voltage response of the piezoelectric generator.

3.9. Flexible alternating current electroluminescent device

A flexible alternating current electroluminescent device (ACEL) is demonstrated using the ultrathin flexible Au/Pt/Au transparent conducting film as both top and bottom electrodes. The main advantage of ACEL devices is their facile fabrication process which can be executed in ambient environment [81]. This is beneficial in extending them to large-area display devices even by simple and cost-effective processes like doctor blading or drop casting. One of the very essential characteristics of an ACEL device is its capability to be made into a very thin device architecture with enhanced flexibility and uniform emission across the whole surface area, leading to wider viewing angles [82]. Fig. 8a shows the flexible electroluminescent device architecture.

The photograph of the fabricated flexible ACEL device using ultrathin Au/Pt/Au film as a transparent conducting electrode and ZnS:Mn as electroluminescent emissive material is shown in Fig. 8b. The working mechanism of ACEL device is as follows: When an AC voltage is applied between the two electrodes, light is emitted by the device due to excitation of luminescence centers within the phosphor material. The entire procedure is divided into four steps: (a) electron injection, (b) electron transport, (c) impact excitation or impact ionization of the luminescence centers and (4) de-excitation of the excited electrons by radiative recombination process (Photon emission) [82]. The ACEL device fabricated using ZnS:Mn emissive layer and Au/Pt/Au ultrathin film electrodes shows orange color emission in the range 590–610 nm [83,84]. Initially, the luminescence flickers at low frequency and is eventually stabilized at higher frequency. The orange ACEL emission begins around 95 V (threshold voltage), and when the applied voltage increases, the intensity of the device increases up to 180 V (saturation voltage). Fig. 8c shows the ACEL emission at 180 V, which is well matched with that of the previously reported ACEL device made from Al and ITO as bottom and top electrodes, respectively [84].

In addition to this, the device is also verified under UV light (365 nm) without any applied voltage as shown in Fig. 8d. Literature reports show that in ACEL devices, the back electrode is given lesser attention for innovation, and in most cases, thick metallic layers possessing high conductivity but no transparency are used in general. In the present case, we have used both the top and bottom electrodes as transparent conducting and flexible ultrathin metallic tri-layers, which is impressive since the flexible ACEL device can emit from both sides of the electrodes, unlike conventional devices that permit only one-side light emission.

Both the PEG and ACEL devices demonstrate that the deposited Au/Pt/Au thin film possesses high electrical conductivity as well as significant transparency, thereby indicating its viability as a potential alternative flexible transparent conducting electrode in a wide range of applications which may be comfortably wrapped around curvilinear surfaces and may respond seamlessly to applied potential or external forces. The flexibility and robustness of the metallic tri-layer electrode may be suitable for long period of operation when used in flexible ACEL devices, making them reliable for real-time usage.

4. Conclusion and outlook

Ultrathin Au/Pt/Au flexible tri-layer film is successfully deposited on

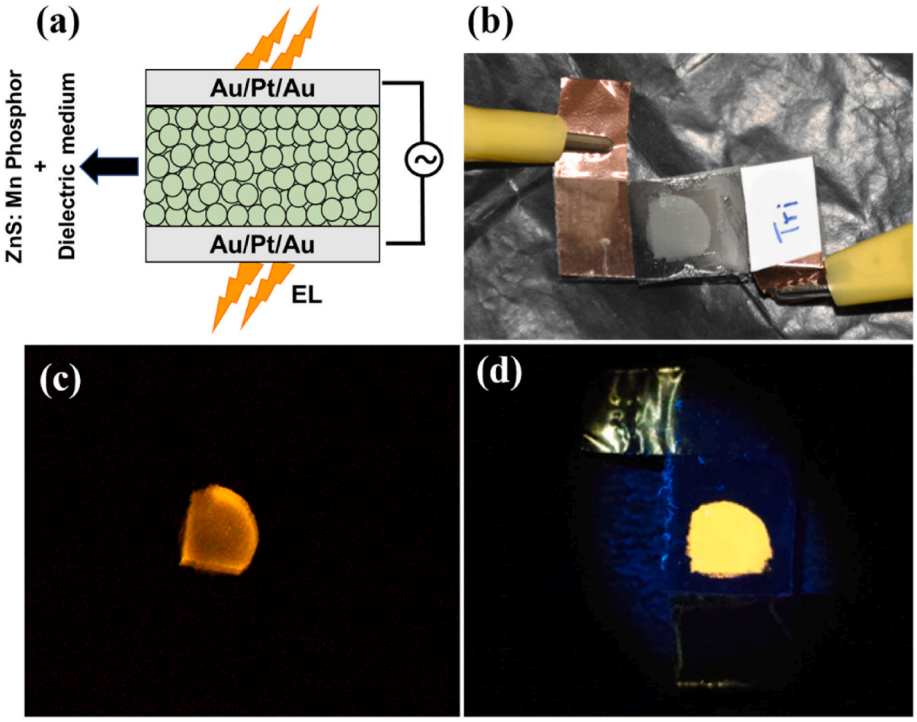

Fig. 8. (a) Alternating current electroluminescent device architecture with Au/Pt/Au film as top and bottom electrodes, (b) Photograph of the electroluminescent device made using Au/Pt/Au flexible transparent film, (c) Response of the device at 180 V, and (d) Response under UV light (365 nm) without any applied voltage.

PET substrate by sputtering technique. Au/Pt/Au film shows maximum transmittance of 55% at 500 nm and a near-flat behavior throughout the spectral range with transmittance between 48% and 55%, revealing its applicability for usage in UV–visible and near infrared regions, and it may be applicable for flexible energy-harvesting applications. It possesses low values of sheet resistance, resistivity, and work function of 62 Ω/□, 3.72 × 10^{-5} Ωcm, and 4.97 eV, respectively. In addition to the appreciable optoelectronic properties, it also exhibits very high mechanical stability of 50,000 bending and twisting cycles, which is far better than that of commercially available ITO, in this range of testing. The commercial ITO shows stability only for a mere 500 bending and twisting cycles. The deposited ultrathin Au/Pt/Au flexible film is demonstrated as an electrode in optoelectronic devices like piezoelectric nanogenerator and alternating current electroluminescent device. The piezoelectric nanogenerator produces nearly 150 mV on applying force by finger tapping. The ACEL device starts producing orange emission at 95 V, and with increase in voltage, the brightness of the device increases up to 180 V. Both the demonstrated devices imply the potential of sputter-deposited ultrathin flexible Au/Pt/Au tri-layer film as a promising electrode system for use in various flexible optoelectronic devices. The ACEL device has an advantage of emitting light from both the top and bottom electrodes, and the transparent top electrode may extend additional functionality of irradiation with UV light in the case of piezoelectric nanogenerator apart from finger tapping. However, further exploration is necessary on an effective strategy to minimize performance failure under mechanical deformations in order to extend the lifetime of the demonstrated optoelectronic devices. The significant retention of optoelectronic properties even after several thousands of mechanical bends and twists indicates the electrical durability of the metallic-tri-layer. Researchers have reported formation of electrical double layers which behave as capacitors in metal-based conductors when combined with dielectric layer [40,81]. Therefore, from this point of view, the ultrathin metal layer has scope for further exploration as electrode system towards realizing bendable micro-supercapacitors. Being highly flexible, the ultrathin tri-layer over 30-μm PET can be tailored simply by cutting it using a pair of scissors or a stencil to make desired electroluminescent patterns of various geometrical shapes and designs for applications like diffuse indoor-lighting in buildings and automobiles, decoration/fashion designing, and also for see-through-flexible electronics. Owing to the low melting point of the 30-μm PET substrate, one can easily laminate it into wearable electronics as well as in safety jackets/traffic signs by suitably altering the phosphor material. Due to the facile and open air-process of the assembly protocol of the demonstrated devices without requirement for high temperature/vacuum, the robust metallic-tri-layer is highly suitable for scalability of various real-time optoelectronic devices for the current and future interactive-display-centric world.

CRediT authorship contribution statement

Reddivari Muniramaiah: Writing – review & editing, Writing – original draft, Visualization, Validation, Software, Methodology, Investigation, Formal analysis, Data curation, Conceptualization. **Jean Maria Fernandes:** Writing – original draft, Visualization, Validation, Formal analysis. **M. Manivel Raja:** Validation, Resources, Formal analysis, Data curation. **Dilli Babu Padmanaban:** Validation, Resources, Formal analysis, Data curation. **P. Supraja:** Validation, Formal analysis, Data curation. **M. Rakshita:** Validation, Formal analysis, Data curation. **Nandarapu Purushotham Reddy:** Validation, Formal analysis, Data curation. **Gouranga Maharana:** Validation, Formal analysis, Data curation. **M. Kovendhan:** Validation, Resources, Formal analysis, Data curation. **Ganapathy Veerappan:** Validation, Resources, Formal analysis, Data curation. **Gangalakurti Laxminarayana:** Validation, Resources, Formal analysis, Data curation. **R. Rakesh Kumar:** Validation, Resources, Formal analysis, Data curation. **D. Haranath:** Validation, Resources, Formal analysis, Data curation. **D. Paul Joseph:** Writing – review & editing, Writing – original draft, Visualization, Validation, Supervision, Resources, Methodology, Investigation, Funding acquisition, Formal analysis, Conceptualization.

Declaration of competing interest

The authors declare that they have no known competing financial interests or personal relationships that could have appeared to influence the work reported in this paper.

Data availability

Data will be made available on request.

Acknowledgement

The authors thank Prof. Davide Mariotti, Ulster University, UK, for Kelvin probe measurements with support from EPSRC award EP/R008841/1. Author M. Rakshita acknowledge the CSIR (Govt. of India) for financial support through the junior research fellowship (#09/0922 (11518)/2021-EMR-1).

Appendix A. Supplementary data

Supplementary data to this article can be found online at https://doi.org/10.1016/j.vacuum.2022.111487.

References

[1] M. Pagliaro, R. Ciriminna, G. Palmisano, BIPV: merging the photovoltaic with the construction industry, Prog. Photovoltaics Res. Appl. 18 (2010) 61–72, https://doi.org/10.1002/PIP.920.

[2] Y. Bi, J. Feng, J. Ji, Y. Chen, Y. Liu, Y. Li, Y.L. Nanoscale, undefined, Ultrathin and Ultrasmooth Au Films as Transparent Electrodes in ITO-free Organic Light-Emitting Devices, Pubs.Rsc.Org., 2016 (n.d.), https://pubs.rsc.org/en/content/articlehtml/2016/nr/c6nr00599c. (Accessed 11 February 2022).

[3] G.M. Wu, H.H. Lin, H.C. Lu, Work function and valence band structure of tin-doped indium oxide thin films for OLEDs, Vacuum 82 (2008) 1371–1374, https://doi.org/10.1016/J.VACUUM.2008.03.038.

[4] T. Dong, J. Simões, Z. Yang, Flexible photodetector based on 2D materials: processing, architectures, and applications, Adv. Mater. Interfac. 7 (2020), 1901657, https://doi.org/10.1002/ADMI.201901657.

[5] M.C. Choi, Y. Kim, C.S. Ha, Polymers for flexible displays: from material selection to device applications, Prog. Polym. Sci. 33 (2008) 581–630, https://doi.org/10.1016/J.PROGPOLYMSCI.2007.11.004.

[6] R. Singh, J. Tharion, S. Murugan, A. Kumar, ITO-free solution-processed flexible electrochromic devices based on PEDOT:PSS as transparent conducting electrode, ACS Appl. Mater. Interfaces 9 (2017) 19427–19435, https://doi.org/10.1021/ACSAMI.6B09476/SUPPL_FILE/AM6B09476_SI_003.AVI.

[7] N. Sezer, M. Koç, A comprehensive review on the state-of-the-art of piezoelectric energy harvesting, Nano Energy 80 (2021), 105567, https://doi.org/10.1016/J.NANOEN.2020.105567.

[8] Y. Li, L.W. Tan, X.T. Hao, K.S. Ong, F. Zhu, L.S. Hung, Flexible top-emitting electroluminescent devices on polyethylene terephthalate substrates, Appl. Phys. Lett. 86 (2005), 153508, https://doi.org/10.1063/1.1900940.

[9] H. Zheng, L. Li, Z. Sun, S. Yu, W. Luo, Preferential orientation, microstructure and functional properties of SnO2:Sb thin film: the effects of post-growth annealing, Appl. Surf. Sci. 362 (2016) 230–236, https://doi.org/10.1016/J.APSUSC.2015.11.230.

[10] D.Y. Park, Y.S. Lee, J.H. Kim, S.J. Lee, S.K. Cho, S.H. Choa, Effects of annealing temperature and hard coating layer on mechanical flexibility of indium tin oxide electrode, Nanosci. Nanotechnol. Lett. 9 (2017) 1185–1189, https://doi.org/10.1166/NNL.2017.2462.

[11] S. Rajendran, J. Qin, F. Gracia, E. Lichtfouse (Eds.), Metal and Metal Oxides for Energy and Electronics, vol. 55, 2021, https://doi.org/10.1007/978-3-030-53065-5.

[12] C. Dai, G. Sun, L. Hu, Y. Xiao, Z. Zhang, Liangti Qu, Z. Correspondence, L. Zhang, B. Qu, Recent Progress in Graphene-based Electrodes for Flexible Batteries, vol. 2, Wiley Online Libr, 2019, pp. 509–526, https://doi.org/10.1002/inf2.12039.

[13] Y. Chen, R.S. Carmichael, T.B. Carmichael, patterned, flexible, and stretchable silver nanowire/polymer composite films as transparent conductive electrodes, ACS Appl. Mater. Interfaces 11 (2019) 31210–31219, https://doi.org/10.1021/ACSAMI.9B11149/SUPPL_FILE/AM9B11149_SI_001.PDF.

[14] H. Kang, S. Jung, S. Jeong, G. Kim, K. Lee, Polymer-metal hybrid transparent electrodes for flexible electronics, Nat. Commun. 61 (6) (2015) 1–7, https://doi.org/10.1038/ncomms7503, 2015.

[15] R. Dover, C. Klein, V. Gutkin, J. Zessin, V. Saik, D. Rotem, O. Millo, D. Porath, G. Sarusi, n-Type doping of triethylenetetramine on single-wall carbon nanotubes for transparent conducting cathodes, ACS Appl. Nano Mater. 4 (2021) 13279–13287, https://doi.org/10.1021/ACSANM.1C02791/SUPPL_FILE/AN1C02791_SI_001.PDF.

[16] W. Zhou, J. Chen, Y. Li, D. Wang, J. Chen, X. Feng, Z. Huang, R. Liu, X. Lin, H. Zhang, B. Mi, Y. Ma, Copper mesh templated by breath-figure polymer films as flexible transparent electrodes for organic photovoltaic devices, ACS Appl. Mater. Interfaces 8 (2016) 11122–11127, https://doi.org/10.1021/ACSAMI.6B01117/SUPPL_FILE/AM6B01117_SI_001.PDF.

[17] X. Li, Y. Meng, R. Fan, S. Fan, C. Dang, X. Feng, J.C. Ho, Y. Lu, High elasticity of CsPbBr3 perovskite nanowires for flexible electronics, Nano Res. 14 (2021) (2021) 4033–4037, https://doi.org/10.1007/S12274-021-3332-0, 1411.

[18] W. Cao, J. Li, H. Chen, J. Xue, Transparent electrodes for organic optoelectronic devices: a review, J. Photon. Energy 4 (2014), 040990, https://doi.org/10.1117/1.jpe.4.040990.

[19] W. Li, H. Zhang, S. Shi, J. Xu, X. Qin, Q. He, K. Yang, W. Dai, G. Liu, Q. Zhou, H. Yu, S.R.P. Silva, M. Fahlman, Recent progress in silver nanowire networks for flexible organic electronics, J. Mater. Chem. C 8 (2020) 4636–4674, https://doi.org/10.1039/C9TC06865A.

[20] B. Myung-Gyu Kang, M.-S. Kim, J. Kim, L. Jay Guo, L.J. Guo, M. Kang, J. Kim, M. Kim, Organic solar cells using nanoimprinted transparent metal electrodes**, (n.d.). https://doi.org/10.1002/adma.200800750.

[21] M.-G. Kang, L.J. Guo, Nanoimprinted semitransparent metal electrodes and their application in organic light-emitting diodes**. https://doi.org/10.1002/adma.200700134, 2007.

[22] K. Tvingstedt, O. Inganäs, Electrode grids for ITO-free organic photovoltaic devices**. https://doi.org/10.1002/adma.200602561, 2007.

[23] R. Gupta, K.D.M. Rao, G.U. Kulkarni, Transparent and flexible capacitor fabricated using a metal wire network as a transparent conducting electrode †. https://doi.org/10.1039/c4ra04632c, 2014.

[24] S. Kiruthika, R. Gupta, A. Anand, A. Kumar, G.U. Kulkarni, Fabrication of oxidation-resistant metal wire network-based transparent electrodes by a spray-roll coating process, ACS Appl. Mater. Interfaces 7 (2015) 27215–27222. https://doi.org/10.1021/ACSAMI.5B08171/ASSET/IMAGES/LARGE/AM-2015-081713_0008.JPEG.

[25] S. De, T.M. Higgins, P.E. Lyons, E.M. Doherty, P.N. Nirmalraj, W.J. Blau, J. J. Boland, J.N. Coleman, Silver nanowire networks as flexible, transparent, conducting films: extremely high DC to optical conductivity ratios. https://doi.org/10.1021/nn900348c, 2009.

[26] J.-Y. Lee, S.T. Connor, Y. Cui, P. Peumans, Solution-processed metal nanowire mesh transparent electrodes, (n.d.). https://doi.org/10.1021/nl073296g.

[27] D.S. Ghosh, L. Martinez, P. Vergani, S. Giurgola, V. Pruneri, Widely transparent electrodes based on ultrathin metals, Opt. Lett. 34 (3) (2009) 325–327, https://doi.org/10.1364/OL.34.000325, 325–327 34.

[28] R.B. Pode, C.J. Lee, D.G. Moon, J.I. Han, Transparent conducting metal electrode for top emission organic light-emitting devices: Ca–Ag double layer, Appl. Phys. Lett. 84 (2004) 4614–4616, https://doi.org/10.1063/1.1756674.

[29] L. Kogut, K. Komvopoulos, Electrical contact resistance theory for conductive rough surfaces separated by a thin insulating film, J. Appl. Phys. 95 (2003) 576, https://doi.org/10.1063/1.1629392.

[30] A. Axelevitch, B. Apter, In-situ investigation of optical transmittance in metal thin films, Thin Solid Films 591 (2015) 261–266, https://doi.org/10.1016/J.TSF.2015.01.046.

[31] D. Leftheriotis, G. Yianoulis, P. Patrikios, Deposition and optical properties of optomised ZnS _ Ag _ ZnS for energy saving applications, Thin Solid Films 306 (1997) 92–99.

[32] H.W. Deng, Y.J. Zhao, C.J. Liang, W.S. Jiang, Y.M. Ning, Effective skin depth for multilayer coated conductor, Prog. Electromagn. Res. M. 9 (2009) 1–8, https://doi.org/10.2528/PIERM09071411.

[33] J. Yun, Ultrathin metal films for transparent electrodes of flexible optoelectronic devices, Adv. Funct. Mater. 27 (2017), 1606641, https://doi.org/10.1002/ADFM.201606641.

[34] X. He, W. Wang, S. Li, Y. Liu, W. Zheng, Q. Shi, X. Luo, Experimental and theoretical analysis of ZnO/Au/ZnO transparent conducting thin films, Vacuum 120 (2015) 17–21, https://doi.org/10.1016/J.VACUUM.2015.06.015.

[35] H.M. Lee, Y.J. Lee, I.S. Kim, M.S. Kang, S.B. Heo, Y.S. Kim, D. Kim, Annealing effect of ZnO/Au/ZnO transparent conductive films, Vacuum 86 (2012) 1494–1498, https://doi.org/10.1016/J.VACUUM.2012.02.041.

[36] Y.S. Kim, J.H. Park, D. Kim, Influence of Au underlayer thickness on the electro-optical properties of ITO/Au layered films deposited by magnetron sputtering on unheated polycarbonate substrates, Vacuum 82 (2008) 574–578, https://doi.org/10.1016/J.VACUUM.2007.08.011.

[37] Z.Y. Nuru, C.J. Arendse, S. Khamlich, M. Maaza, Optimization of AlxOy/Pt/AlxOy multilayer spectrally selective coatings for solar–thermal applications, Vacuum 86 (2012) 2129–2135, https://doi.org/10.1016/J.VACUUM.2012.06.012.

[38] C. Surya Prakasarao, P. Hazarika, S.D. Dsouza, J.M. Fernandes, M. Kovendhan, R. Arockia Kumar, D. Paul Joseph, Investigation of ultra-thin and flexible Au–Ag–Au transparent conducting electrode, Curr. Appl. Phys. 20 (2020) 1118–1124, https://doi.org/10.1016/J.CAP.2020.06.016.

[39] J. Zhu, D. Han, X. Wu, J. Ting, S. Du, A.C. Arias, Highly flexible transparent micromesh electrodes via blade-coated polymer networks for organic light-emitting diodes, ACS Appl. Mater. Interfaces 12 (2020) 31687–31695, https://doi.org/10.1021/ACSAMI.0C07299/SUPPL_FILE/AM0C07299_SI_001.PDF.

[40] C. Ji, D. Liu, C. Zhang, L. Jay Guo, Ultrathin-metal-film-based transparent electrodes with relative transmittance surpassing 100, Nat. Commun. 11 (2020), https://doi.org/10.1038/S41467-020-17107-6.

[41] L. Shao, X. Zhao, S. Gu, Y. Ma, Y. Liu, X. Deng, H. Jiang, W. Zhang, Pt thin-film resistance temperature detector on flexible Hastelloy tapes, Vacuum 184 (2021), 109966, https://doi.org/10.1016/J.VACUUM.2020.109966.

[42] S. Iwatsubo, Morphology and characteristics of ultrathin Au films with ultraviolet transparency and conductivity deposited by dual ion beam sputtering, Vacuum 74 (2004) 631–636, https://doi.org/10.1016/J.VACUUM.2004.01.037.
[43] H. Chander, V. Shanker, D. Haranath, S. Dudeja, P. Sharma, Characterization of ZnS:Cu, Br electroluminescent phosphor prepared by new route, Mater. Res. Bull. 38 (2003) 279–288, https://doi.org/10.1016/S0025-5408(02)01027-9.
[44] undefined J. Wang, C. Yan, G. Cai, M. Cui, E.-A. A.L., Extremely Stretchable Electroluminescent Devices with Ionic Conductors, vol. 28, Wiley Online Libr, 2016, pp. 4490–4496, https://doi.org/10.1002/adma.201504187, 2015.
[45] M. He, K. Zhang, G. Chen, J. Tian, B. Su, Ionic gel paper with long-term bendable electrical robustness for use in flexible electroluminescent devices, ACS Appl. Mater. Interfaces 9 (2017) 16466–16473, https://doi.org/10.1021/ACSAMI.7B02433/SUPPL_FILE/AM7B02433_SI_001.PDF.
[46] J. Hou, M. Liu, H. Zhang, Y. Song, X. Jiang, A. Yu, L. Jiang, B. Su, Healable green hydrogen bonded networks for circuit repair, wearable sensor and flexible electronic devices, J. Mater. Chem. A. 5 (2017) 13138–13144, https://doi.org/10.1039/C7TA03100A.
[47] R. Tong, G. Chen, J. Tian, M. He, Highly transparent, weakly hydrophilic and biodegradable cellulose film for flexible electroluminescent devices, Carbohydr. Polym. 227 (2020), 115366, https://doi.org/10.1016/J.CARBPOL.2019.115366.
[48] Z. Jiang, K. Fukuda, X. Xu, S. Park, D. Inoue, H. Jin, M. Saito, I. Osaka, K. Takimiya, T. Someya, Reverse-offset printed ultrathin Ag mesh for robust conformal transparent electrodes for high-performance organic photovoltaics, Adv. Mater. 30 (2018), 1707526, https://doi.org/10.1002/ADMA.201707526.
[49] K.G. Kostov, A.L.R. Dos Santos, P.A.P. Nascente, M.E. Kayama, R.P. Mota, Modification of polyethylene terephthalate by atmospheric pressure dielectric barrier discharge (DBD) in view of improving the polymer wetting properties, J. Phys. Conf. Ser. 356 (2012), 012006, https://doi.org/10.1088/1742-6596/356/1/012006.
[50] Y.W. Mo, D.E. Savage, B.S. Swartzentruber, M.G. Lagally, Kinetic pathway in Stranski-Krastanov growth of Ge on Si(001), Phys. Rev. Lett. 65 (1990) 1020–1023, https://doi.org/10.1103/PHYSREVLETT.65.1020.
[51] C.L. Hsiao, J. Palisaitis, P.O.Å. Persson, M. Junaid, E.A. Serban, P. Sandström, L. Hultman, J. Birch, Nucleation and core-shell formation mechanism of self-induced InxAl1−xN core-shell nanorods grown on sapphire substrates by magnetron sputter epitaxy, Vacuum 131 (2016) 39–43, https://doi.org/10.1016/J.VACUUM.2016.05.022.
[52] L. Zhang, R. Dillert, D. Bahnemann, M. Vormoor, Photo-induced hydrophilicity and self-cleaning: models and reality, Energy Environ. Sci. 5 (2012) 7491–7507, https://doi.org/10.1039/C2EE03390A.
[53] T.T. Chau, W.J. Bruckard, P.T.L. Koh, A.V. Nguyen, A review of factors that affect contact angle and implications for flotation practice, Adv. Colloid Interface Sci. 150 (2009) 106–115, https://doi.org/10.1016/J.CIS.2009.07.003.
[54] C.S. Prakasarao, S.D. D'Souza, P. Hazarika, S.N. Karthiselva, R. Ramesh Babu, M. Kovendhan, R.A. Kumar, D.P. Joseph, Fabrication and stability investigation of ultra-thin transparent and flexible Cu-Ag-Au tri-layer film on PET, AIP Conf. Proc. 1942 (2018), 080010, https://doi.org/10.1063/1.5028844.
[55] A. Axelevitch, B. Gorenstein, G. Golan, Investigation of optical transmission in thin metal films, Phys. Procedia 32 (2012) 1–13, https://doi.org/10.1016/J.PHPRO.2012.03.510.
[56] C.P. Liu, Y. Foo, M. Kamruzzaman, C.Y. Ho, J.A. Zapien, W. Zhu, Y.J. Li, W. Walukiewicz, K.M. Yu, Effects of free carriers on the optical properties of doped CdO for full-spectrum photovoltaics, Phys. Rev. Appl. 6 (2016), 064018, https://doi.org/10.1103/PHYSREVAPPLIED.6.064018/FIGURES/11/MEDIUM.
[57] M. Fox, G.F. Bertsch, Optical properties of solids, Cit. Am. J. Phys. 70 (2002) 1269, https://doi.org/10.1119/1.1691372.
[58] H. Peng, W. Dang, J. Cao, Y. Chen, D. Wu, W.Z.-N. undefined, Topological insulator nanostructures for near-infrared transparent flexible electrodes, Nature.Com (2012) (n.d.), https://www.nature.com/articles/nchem.1277. (Accessed 11 February 2022).
[59] A.D. Laforge, A. Frenzel, B.C. Pursley, T. Lin, X. Liu, J. Shi, D.N. Basov, Optical characterization of Bi2Se3 in a magnetic field: infrared evidence for magnetoelectric coupling in a topological insulator material, Phys. Rev. B Condens. Matter 81 (2010), 125120, https://doi.org/10.1103/PHYSREVB.81.125120/FIGURES/10/MEDIUM.
[60] Y.-G. Bi, Y.-F. Liu, X.-L. Zhang, D. Yin, W.-Q. Wang, J. Feng, H.-B. Sun, Y.-G. Bi, Y.-F. Liu, X.-L. Zhang, D. Yin, J. Feng, -B.H. Sun, -Q.W. Wang, Ultrathin metal films as the transparent electrode in ITO-free organic optoelectronic devices, Adv. Opt. Mater. 7 (2019), 1800778, https://doi.org/10.1002/ADOM.201800778.
[61] R.S. Markiewicz, L.A. Harris, Two-dimensional resistivity of ultrathin metal films, Phys. Rev. Lett. 46 (1981) 1149, https://doi.org/10.1103/PhysRevLett.46.1149.
[62] C.S. Prakasarao, S.D. D'Souza, P. Hazarika, S.N. Karthiselva, R. Ramesh Babu, M. Kovendhan, R.A. Kumar, D.P. Joseph, Fabrication and stability investigation of ultra-thin transparent and flexible Cu-Ag-Au tri-layer film on PET, AIP Conf. Proc. 1942 (2018), 080010, https://doi.org/10.1063/1.5028844.
[63] Y. Muraoka, N. Takubo, Z. Hiroi, Photoinduced conductivity in tin dioxide thin films, J. Appl. Phys. 105 (2009), 103702, https://doi.org/10.1063/1.3126713.
[64] W. Melitz, J. Shen, A.C. Kummel, S. Lee, Kelvin probe force microscopy and its application, Surf. Sci. Rep. 66 (2011) 1–27, https://doi.org/10.1016/J.SURFREP.2010.10.001.
[65] J. Hölzl, F.K. Schulte, Work Function of Metals, 1979, pp. 1–150, https://doi.org/10.1007/BFB0048919.
[66] R. Schlaf, H. Murata, Z.H. Kafafi, Work function measurements on indium tin oxide films, J. Electron. Spectrosc. Relat. Phenom. 120 (2001) 149–154, https://doi.org/10.1016/S0368-2048(01)00310-3.
[67] K. Sugiyama, H. Ishii, Y. Ouchi, K. Seki, Dependence of indium–tin–oxide work function on surface cleaning method as studied by ultraviolet and x-ray photoemission spectroscopies, J. Appl. Phys. 87 (1999) 295, https://doi.org/10.1063/1.371859.
[68] Y. Park, V. Choong, Y. Gao, B.R. Hsieh, C.W. Tang, Work function of indium tin oxide transparent conductor measured by photoelectron spectroscopy, Appl. Phys. Lett. 68 (1998) 2699, https://doi.org/10.1063/1.116313.
[69] T. Kugler, W.R. Salaneck, H. Rost, A.B. Holmes, Polymer band alignment at the interface with indium tin oxide: consequences for light emitting devices, Chem. Phys. Lett. 310 (1999) 391–396, https://doi.org/10.1016/S0009-2614(99)00824-6.
[70] Z. Suo, E.Y. Ma, H. Gleskova, S. Wagner, Mechanics of rollable and foldable film-on-foil electronics, Appl. Phys. Lett. 74 (1999) 1177, https://doi.org/10.1063/1.123478.
[71] D. Yin, J. Feng, N.R. Jiang, R. Ma, Y.F. Liu, H.B. Sun, Two-dimensional stretchable organic light-emitting devices with high efficiency, ACS Appl. Mater. Interfaces 8 (2016) 31166–31171, https://doi.org/10.1021/ACSAMI.6B10328/SUPPL_FILE/AM6B10328_SI_004.AVI.
[72] A.M. Badkoobehhezaveh, E. Hopmann, A.Y. Elezzabi, Flexible multicolor electroluminescent devices on cellulose nanocrystal platform, Adv. Eng. Mater. 22 (2020), 1901452, https://doi.org/10.1002/ADEM.201901452.
[73] G. Zhao, S.M. Kim, S.G. Lee, T.S. Bae, C.W. Mun, S. Lee, H. Yu, G.H. Lee, H.S. Lee, M. Song, J. Yun, Bendable solar cells from stable, flexible, and transparent conducting electrodes fabricated using a nitrogen-doped ultrathin copper film, Adv. Funct. Mater. 26 (2016) 4180–4191, https://doi.org/10.1002/ADFM.201600392.
[74] D. Zhao, C. Zhang, H. Kim, L.J. Guo, High-performance Ta2O5/Al-doped Ag electrode for resonant light harvesting in efficient organic solar cells, Adv. Energy Mater. 5 (2015), 1500768, https://doi.org/10.1002/AENM.201500768.
[75] Y.G. Bi, F.S. Yi, J.H. Ji, C. Ma, W.Q. Wang, J. Feng, H.B. Sun, Ultrathin Au electrodes based on a hybrid nucleation layer for flexible organic light-emitting devices, IEEE Trans. Nanotechnol. 17 (2018) 1077–1081, https://doi.org/10.1109/TNANO.2018.2860055.
[76] Y.G. Bi, J. Feng, J.H. Ji, Y. Chen, Y.S. Liu, Y.F. Li, Y.F. Liu, X.L. Zhang, H.B. Sun, Ultrathin and ultrasmooth Au films as transparent electrodes in ITO-free organic light-emitting devices, Nanoscale 8 (2016) 10010–10015, https://doi.org/10.1039/C6NR00599C.
[77] D. Yin, Z.Y. Chen, N.R. Jiang, Y.F. Liu, Y.G. Bi, X.L. Zhang, W. Han, J. Feng, H. B. Sun, Highly transparent and flexible fabric-based organic light emitting devices for unnoticeable wearable displays, Org. Electron. 76 (2020), 105494, https://doi.org/10.1016/J.ORGEL.2019.105494.
[78] X. Guo, X. Liu, F. Lin, H. Li, Y. Fan, N. Zhang, Highly conductive transparent organic electrodes with multilayer structures for rigid and flexible optoelectronics, Sci. Rep. 51 (5) (2015) 1–9, https://doi.org/10.1038/srep10569, 2015.
[79] Y. Manjula, R. Rakesh Kumar, P.M. Swarup Raju, G. Anil Kumar, T. Venkatappa Rao, A. Akshaykranth, P. Supraja, Piezoelectric flexible nanogenerator based on ZnO nanosheet networks for mechanical energy harvesting, Chem. Phys. 533 (2020), 110699, https://doi.org/10.1016/j.chemphys.2020.110699.
[80] J. Kaur, · Harminder Singh, Synthesis and fabrication of zinc oxide nanostrands based piezoelectric nanogenerator, J. Mater. Sci. Mater. Electron. 30 (2019) 4437–4445, https://doi.org/10.1007/s10854-019-00732-3.
[81] M. Bredol, H.S. Dieckhoff, Materials for powder-based AC-electroluminescence, Materials 3 (2010) 1353–1374, https://doi.org/10.3390/MA3021353, 3 (2010) 1353–1374.
[82] W.A.D.M. Jayathilaka, A. Chinnappan, J.N. Tey, J. Wei, S. Ramakrishna, Alternative current electroluminescence and flexible light emitting devices, J. Mater. Chem. C 7 (2019) 5553–5572, https://doi.org/10.1039/C9TC01267B.
[83] Y. Tong, Z. Jiang, C. Wang, Y. Xin, Z. Huang, S. Liu, C. Li, Effect of annealing on the morphology and properties of ZnS:Mn nanoparticles/PVP nanofibers, Mater. Lett. 62 (2008) 3385–3387, https://doi.org/10.1016/J.MATLET.2008.03.016.
[84] S. Tiwari, S. Tiwari, B.P. Chandra, Characteristics of a.c. electroluminescence in thin film ZnS : Mn display devices, J. Mater. Sci. Mater. Electron. 15 (2004) (2004) 569–574, https://doi.org/10.1023/B:JMSE.0000036034.60370.42, 159.